D-shaped surface plasmon photonic crystal fiber temperature sensor

Shutao Wang
Yanshan University
Yuhong Lu (1002921386@qq.com)
Yanshan University
Wenbo Ma
Yanshan University
Na Liu
Yanshan University
Shuanhe Fan
Yanshan University

Research Article

Keywords: Surface plasmon resonance, Photonic crystal fiber, Temperature sensor, polished D-shaped flat

Posted Date: May 5th, 2022

DOI: https://doi.org/10.21203/rs.3.rs-1604019/v1

D-shaped surface plasmon photonic crystal fiber temperature sensor

Shutao Wang [1], Yuhong Lu [1]*, Wenbo Ma [1], Na Liu [1], Shuanhe Fan [1]

Measurement Technology and Instrumentation Key Lab of Hebei Province, Yanshan University, Qinhuangdao 066004, Hebei, China

*Corresponding author:1002921386@qq.com

Abstract This work presents a D-shaped photonic crystal fiber temperature sensor based on surface plasmon resonance with high sensitivity and high figure of merit. To enhance surface plasmon resonance, the gold film is deposited on the polished flat of D-shaped photonic crystal fiber. Ethanol and chloroform are employed as temperature-sensitive materials, which are placed on the outside of the fiber to detect temperature changes. When the phase-matching condition is met, the core mode couples with the surface plasma mode, resulting in energy transfer. The finite element method is used to perform all numerical simulations of sensor characteristics in the COMSOL software. The results show that the highest sensitivity of the sensor can reach 6.36 nm/°C, and the maximum figure of merit (FOM) is 0.3440/°C between -5 ℃ and 60 °C. To our knowledge, the achieved sensing characteristics are significantly better than those of the current PCF temperature sensors. Furthermore, excellent linearity with a polynomial fit R^2 of up to 0.9981. The proposed sensor has exceptional performance in terms of temperature detection range, sensitivity, FOM and fabrication, making it suitable for a wide variety of biochemical and medical applications.

Key words Surface plasmon resonance; Photonic crystal fiber; Temperature sensor; polished D-shaped flat

OCIS codes 060.5295; 240.6680; 280.4788; 280.6780

Introduction

Photonic crystal fiber (PCF) exhibits superior properties owing to its unique structure, including infinite single-mode transmission, high nonlinearity, controllable birefringence and tunable dispersion [1-3]. In recent years, PCF-based temperature sensors have gained considerable interest due to their small size, light weight, and distant sensing capability. Numerous types of PCF temperature sensors have already appeared to date, such as long period grating (LPG), mode coupling, Sagnac interferometer and surface plasmon resonance [4-10]. Du C et al. [5] proposed a method for measuring temperature using an isopropanol-filled PCF with a long period grating, the maximum sensitivity of sensor in the range of 20-50 ℃ is 1.356 nm/℃. However, LPG-based sensors are expensive because of the need for high-power lasers in fabrication. A all-fiber Sagnac interferometer temperature sensor with high sensitivity of 1.65 nm/°C was reported by Li et al [6], but temperature detection range of only 25-33 °C. Liu Q et al. [7] demonstrated a PCF temperature sensor with a larger sensing range from 20 ℃ to 80 °C based on the coupling of liquid core and defect mode, while the sensitivity is -1.9 nm/°C and the FOM can go as low as -0.035/°C. A temperature sensor with polarization-insensitive based on liquid-filled PCF was proposed by Abbasi M et al. [10] and obtained the sensitivity of -1.96 nm/°C in both x and y polarization directions. Additionally, the FOM of sensor is up to 0.272/℃, but sensitivity should be improved.

Surface plasmon resonance (SPR) technology is one of the major achievements of modern optics. SPR is extremely sensitive and precise to changes in the refractive index of the surrounding medium, so it is frequently used in the design of various refractive index sensors. Due to the fact that temperature has an effect on the refractive index change of the medium, the temperature sensor based on SPR has become a research hotspot in recent years [11-14]. In 2012, Peng Y et al. [15] first achieved an SPR-based PCF temperature sensor, in which the PCF air holes were covered by gold films for SPR response. A high-sensitivity SPR-PCF temperature sensor with a central liquid crystal-filled air hole and gold wires filling of some air holes in the layer was recorded by Hameed et al. [16], the sensitivity can reach up to 10 nm/°C between 30 ℃ and 50 ℃. Bo Han et al. [17] simultaneously measured temperature and strain in two symmetrical PCF holes coated with golden layer, one of which was permeated with a temperature-sensitive liquid. This sensor exhibited sensitivity of -6.83 nm/°C with a narrow temperature range of 20-30 ℃. Clearly, the SPR-PCF temperature sensor has a higher sensitivity. However, the temperature range of the above sensors are limited and only the sensitivity is studied. Thus, it is critical to investigate how to concurrently increase the performance of SPR-PCF temperature sensor across a wide temperature range, including sensitivity, FOM, and so on. The PCF air holes are small, making it extremely difficult to place temperature-sensitive materials and metal films in them. Therefore, simplifying the design and fabrication of PCF is important.

In this work, a multi-channel D-shaped PCF temperature sensor based on SPR is designed and studied by finite element method. The arrangement of air holes is only two layers, which simplifies the structure design. Gold has high stability and is difficult to oxidize, so it is deposited on the D-shaped surface to excite plasmon resonance. Here, the ethanol and chloroform are placed outside of PCF as the temperature sensitive liquid. Therefore, the problems associated with covering the film and filling liquid in the air holes can be efficiently overcome. Through simulation, we firstly analyze the parameters about sensitivity and FOM of the sensor and attain excellent sensing performance. Moreover, the optimization of structural parameters about gold film thickness and the distance from

center to polished flat of PCF are investigated. Comparing and analyzing various PCF temperature sensors at last, our sensor exhibits superior sensing performance and is very competitive in the field of temperature sensing.

Structure design and basic theory

The cross-sectional view of the designed SPR-PCF temperature sensor is shown in Fig. 1, modal analysis is conducted in the X-Y plane, and incident light along the Z direction. The sensor structure consists of two layers of cladding air holes. The air holes with diameters d, d_1 and d_2 are arranged in a regular hexagon lattice, and the pitch of lattice is Λ. On the side close to the metal film are two air holes with a diameter of d_3, and the distance to the center of the air hole below is Λ/1.1. Here, the fiber radius is r, the side polished flat coated with gold film of thickness t height from fiber core is h. There are fewer air holes on the side near the gold film, which enable multi-channel transmission of core energy. Temperature-sensitive liquid mixed with ethanol and chloroform at a ratio of 1:1 is placed on the outer layer. Chloroform has a high thermal coefficient but a large refractive index. Thus, adding ethanol to reduce the refractive index of the liquid. Outermost layer is a perfectly matched layer, which is used to absorb the radiation energy and ensure the accuracy of the calculation. Due to the fact that the air holes are closely spaced, the PCF designed can be fabricated using high-precision ultrasonic drilling [18].

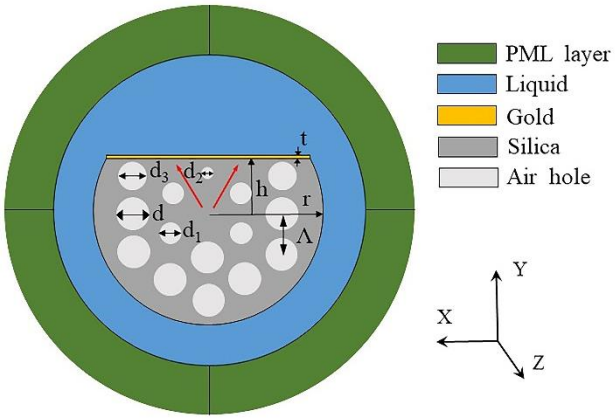

Fig.1 Schematic cross-section of proposed PCF-SPR temperature sensor with Λ=2.5 μm, h=3.5 μm, d=2 μm, d_1=1.5 μm, d_2=0.75 μm, d_3=1.8 μm, r=6.5 μm, t=30 nm

The background material of the temperature sensor is fused silica, and its refractive index can be obtained from the Sellmeier equation [19]

$$n^2(\lambda,T)=\left(1.31552+6.90754\times10^{-6}T\right)+\frac{\left(0.788404+23.5835\times10^{-6}T\right)\lambda^2}{\lambda^2-\left(0.0110199+0.584758\times10^{-6}T\right)}+\frac{\left(0.91316+0.548368\times10^{-6}T\right)\lambda^2}{\lambda^2-100} \quad (1)$$

where incident light wavelength λ is in microns and temperature T is in degree Celsius. The dielectric constant of the gold film on the polished surface is analyzed by the Drude-Lorentz model [20]

$$\varepsilon_{Au}=\varepsilon_\infty-\frac{{\omega_D}^2}{\omega\left(\omega+i\gamma_D\right)}-\frac{\Delta\varepsilon\cdot\Omega_L}{\left(\omega^2-{\Omega_L}^2\right)+i\Gamma_L\omega} \quad (2)$$

Here, ε_∞=5.9673 is the permittivity of gold at high frequency. ω is the angular frequency of guided light, ω_D and γ_D represent the plasma and damping frequency, respectively. $\omega_D/2\pi$ =2113.6THz, $\gamma_D/2\pi$ =15.92 THz. Ω_L and Γ_L are frequency and spectral width of Lorentz oscillators. $\Omega_L/2\pi$ =650.07 THz, $\Gamma_L/2\pi$ =104.86 THz, $\Delta\varepsilon$ =1.09 can be interpreted as a weighting factor. Since temperature-sensitive liquid is more sensitive to temperature than metal, the temperature properties of gold film are ignored [21]. Thermosensitive liquid is a mixture of ethanol and chloroform, and its refractive index [22] can be expressed as

$$n = x\% \times \left[n_{\text{chloroform}} \left| T = 20℃ + \frac{dn_{\text{chloroform}}}{dT} \times (T - 20) \right. \right] + (100\text{-}x)\% \times \left[n_{\text{ethanol}} \left| T = 20℃ + \frac{dn_{\text{ethanol}}}{dT} \times (T - 20) \right. \right] \tag{3}$$

where x% and (100-x)% indicate the proportions of ethanol and chloroform, respectively, and the ratio in the text is 1:1. Material dispersion of liquid is neglected, supposing the refractive indices of ethanol and chloroform are 1.36048 and 1.43136 at T = 20 °C. dn/dT represents the thermo-optic coefficient, and the liquid of thermo-optic coefficient are -3.94×10^{-4}/℃ and -6.328×10^{-4}/℃ [23,24].

When the core and surface plasmon polariton (SPP) modes of the SPR-PCF temperature sensor are coupled at a specific wavelength, SPR occurs when the excitation of the free electrons of the metal by the incident light's evanescent field, transferring energy from the core mode to the SPP mode [25]. This particular wavelength is referred to as the phase matching point and the resonance wavelength. As a result, a loss peak appears at the resonance wavelength. When the temperature varies, the effective refractive index of core mode and SPP mode vary, resulting in a shift in the resonant wavelength. Thus, temperature detection can be achieved based on the resonance wavelength.

The temperature upper limit in this work is set at 60 °C based on the boiling point of the blended liquid. At a temperature of -5 °C, there is an almost completely coupled resonance between the core mode and the SPP mode, because the loss of resonance peaks decreases with decreasing temperature starting at -5 ℃. Hence, temperature detection range from -5 ℃ to 60 ℃ is selected.

Results and discussions

Analysis of electric field distribution, dispersion relations and mode losses

The proposed sensor is simulated using the full vector finite element method in COMSOL software. At T = -5 ℃, the temperature sensor is numerically calculated and analyzed in the 0.82 μm to 0.9 μm wavelength range. Fig. 2 shows the electric field distribution diagram for the x-pol and y-pol core modes, the y-pol SPP mode, and the y-pol coupling resonance at various wavelengths. As can be seen in Fig. 2 (d) and (e), when the wavelength λ = 0.8568 μm, electric field distribution of the x-pol core mode is almost unchanged, while the y-pol core mode and the SPP mode are phase-matched, the majority of energy in the core is transferred to the gold film, resulting in a strong SPR effect. Fig. 3 displays the loss spectra of core mode and the dispersion relations of y-pol core mode and plasmon mode at T = -5 ℃. It can be seen from the figure that the loss of the y-pol core mode is high and exhibits a clear peak between 0.82 μm and 0.9 μm, whereas the x-pol core mode loss is

mild and stable. The *y*-pol core mode experienced stronger interaction with the SPP mode, and the sensitivity was higher, so the *y*-pol mode is considered for the entire sensing process. According to Fig. 3, the real part of the effective refractive index of the *y*-pol core mode and the SPP mode are coincident at a wavelength of 0.8568 μm, and the value of loss peak of *y*-pol core mode is up to 317.51 dB/cm. The calculation formula of the loss can be defined as[26]

$$\alpha\left(\mathrm{dB/cm}\right)=8.686\times\frac{2\pi}{\lambda}\times\mathrm{Im}\left(n_{eff}\right)\times10^{4} \tag{4}$$

Where Im(n_{eff}) represent the imaginary part of the effective refractive index.

Fig. 4 (a) shows the loss spectra of the *y*-pol core mode at -5-60 °C. When the temperature changes from 60 °C to -5 °C, the refractive index of the mixture of temperature-sensitive liquid is approaching that of the core, so the coupling between the core mode and the SPP mode has been increasing which leads to the red-shifted of resonance wavelengths. Simultaneously, the value of the loss peak increases significantly as the temperature decreases. When nearly all of the energy in the *y*-pol core mode is transferred to the SPP mode, the coupling between them changes from incomplete to complete, then the loss of core mode and the SPP mode will reverse. As shown in Fig. 4 (b), when the temperature is changed from 0 °C to -5 °C, the loss peak increases and the resonance wavelength redshifts, but the opposite occurs when the temperature is changed from -5 °C to -15 °C. So it can be concluded that at -5 °C, the coupling between the *y*-pol core mode and the SPP mode is nearly complete, resulting in a high coupling efficiency[27], and the core mode loss reaches its maximum value.

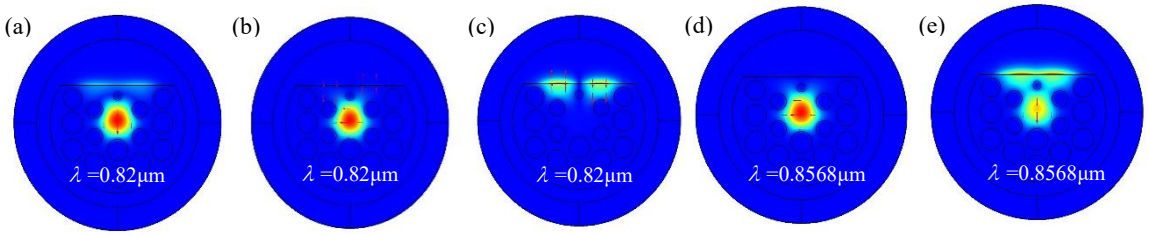

Fig. 2 Electric field distributions of the (a) and (e) x-pol core mode, (b) y-pol core mode, (c) y-pol SPP mode, (d) y- pol coupling mode at T = -5℃

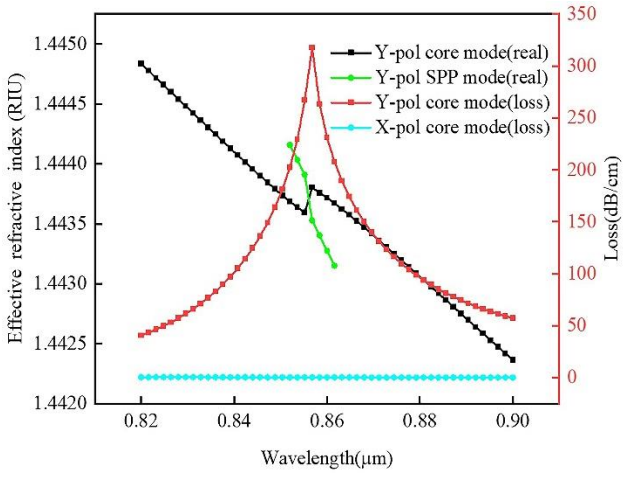

Fig. 3 Loss spectra of the core modes and the dispersion relations of y-polarized core mode and plasma mode at T = -5℃

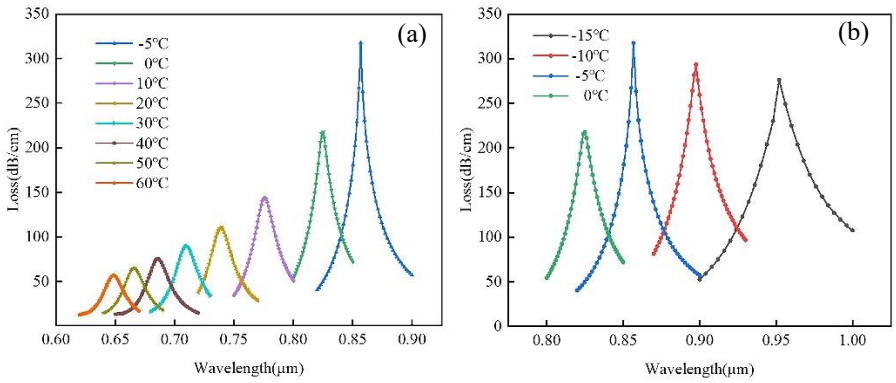

Fig. 4 Loss spectra of the y-pol core mode in the temperature range (a) from -5 ℃ to 60 ℃ and (b) from -15 ℃ to 0 ℃

Analysis of sensor sensing performance

In the detection range, the sensor performances are analyzed in terms of sensitivity, figure of merit (FOM) and the linearity of resonance wavelength. Sensitivity is an important parameter for a temperature sensor, and it is calculated using the wavelength interrogation method. The sensitivity of the sensor is investigated between -5 ℃ and 60 ℃ in this article and the expression can be written as[28]

$$S\left(\text{nm}/^{\circ}\text{C}\right)=\frac{\Delta\lambda_{\text{peak}}}{\Delta T} \tag{5}$$

where $\Delta\lambda_{\text{peak}}$ and ΔT represent the shifting distance of the resonance wavelength and change of the temperature. From Fig. 4, we can obtain the variation of the λ_{peak} (resonance wavelength) and T (temperature), the sensitivity can be calculated as shown in Table 1. It can be seen from the table that the sensor has a maximum sensitivity of 6.36 nm/°C at -5 °C, which is better than a range of previously designed PCF temperature sensors.

The figure of merit (FOM) is another critical sensor parameter, it is defined as the ratio of the sensitivity to the full-width at half-maximum (FWHM), with the following expression[29]

$$FOM\left(^{\circ}\text{C}^{-1}\right)=\frac{S}{FWHM} \tag{6}$$

The sharp resonant response (lower FWHM) can effectively filters out spectral noise, resulting in a greater signal to noise ratio for the received signal. Therefore, higher sensitivity as well as lower FWHM are important directions to improve detection accuracy. In many circumstances, high sensitivity and a high FOM within the temperature sensor's wide detection range cannot be obtained simultaneously. In this paper the proposed sensor achieves a narrow FWHM value of the core mode loss at -5 °C, hence improving both sensitivity and FOM. The FOM and FWHM values of the sensor at various temperatures are listed in Table 1 and the highest FOM of 0.3440/°C, that is also indicative of increased performance. According to Fig. 5 (a), the FOM reaches its highest value when the FWHM is the lowest. Fig. 5 (b) shows quadratic fitting of the loss peak wavelengths changing with temperature between -5 °C and 60 °C, which gives a satisfactory linearity with polynomial fit R^2 up to 0.9981.

Table1 Sensing performance of PCF-SPR temperature sensor in the temperature range from -5 ℃ to 60 ℃

T(℃)	λ_{peak} (nm)	$\Delta\lambda_{peak}$ (nm)	S (nm/℃)	FWHM (nm)	FOM ($℃^{-1}$)
-5	856.8	31.8	6.36	18.49	0.3440
0	825	49	4.9	26.35	0.1860
10	776	37	3.7	29.62	0.1249
20	739	29	2.9	29.06	0.0998
30	710	24	2.4	27.98	0.0858
40	686	20	2	26.88	0.0744
50	666	18	1.8	25.94	0.0694
60	648	—	—	25.14	—

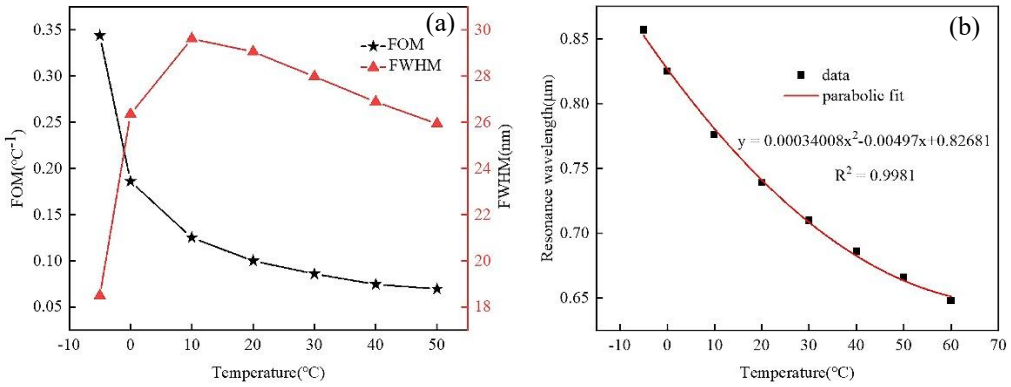

Fig. 5 Variations of the (a) FOM and FWHM values and (b) quadratic fitting of resonance Wavelength for different temperatures

Optimization of the structural parameters

When structural parameters are changed, the temperature sensing characteristics are altered as well. This section investigates the effect of gold film thickness (t) and the distance from fiber core to polished flat (h) on sensing properties in order to optimize sensing performance. The core mode loss spectra of t = 20 nm and t = 25 nm at the temperature of -5~60 ℃ are plotted in Fig. 6 (a) and (b), and the corresponding sensitivity can be calculated. Fig. 6 (c) depicts the sensitivity with the variation of temperature under different gold film thicknesses, it can be observed that when t = 30 nm, the sensing sensitivity is the highest. Fig. 6 (d) and (e) are the FOM and FWHM values versus temperature at t = 20 nm and 25 nm, respectively. Their figures of merit (FOM) are 0.2620/°C and 0.2537/°C, which are both smaller than the 0.3440/°C at t = 30 nm. Therefore, gold film thickness t is optimized to 30 nm with consideration of high sensitivity and FOM.

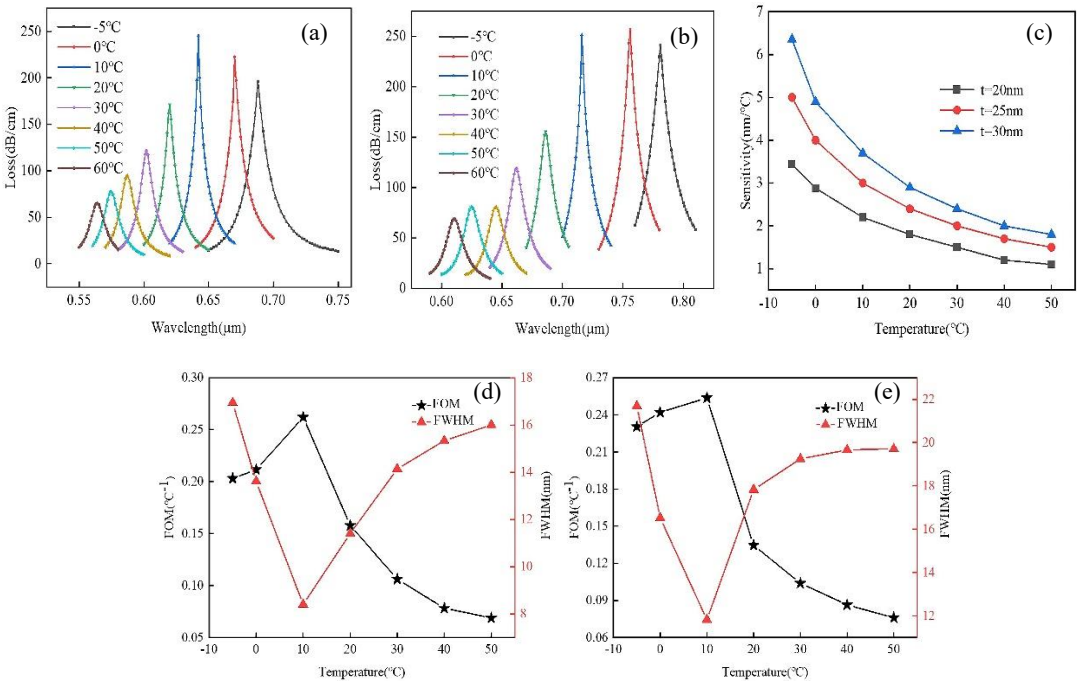

Fig. 6 The core mode loss spectra of (a) t = 20 nm and (b) t = 25 nm, (c) the sensitivity versus temperature with different value of t, FOM and FWHM values at (d) t = 20 nm and (e) t = 25 nm for different temperature

The distance from fiber core to polished flat (h) has an effect on the efficiency with which energy in the core is transmitted to the gold layer, and then affecting sensing performance. Fig. 7 (a) and (b) show the core mode loss spectra of h = 3.4 μm and 3.6 μm at the temperature of -5~60 ℃. The sensitivity with the variation of temperature at h = 3.4 μm, 3.5 μm and 3.6 μm are plotted in Fig. 7 (c). And their maximum sensitivities are 5.8 nm/°C, 6.36 nm/°C and 6.8 nm/°C, respectively. Moreover, from Fig. 5 (a), Fig. 7 (d) and (e), it can be obtained that the FOM of different value of h, which are 0.3538/°C, 0.3440/°C and 0.3234/°C. As illustrated in Fig. 7 (c) and (f), when h=3.4 μm, the sensing sensitivity is lowest but the FOM is highest, while h=3.6 μm is the opposite. Both the sensitivity and FOM are relatively high at h=3.5 μm. As a result, h is optimized to 3.5 μm for getting better temperature sensing characteristics.

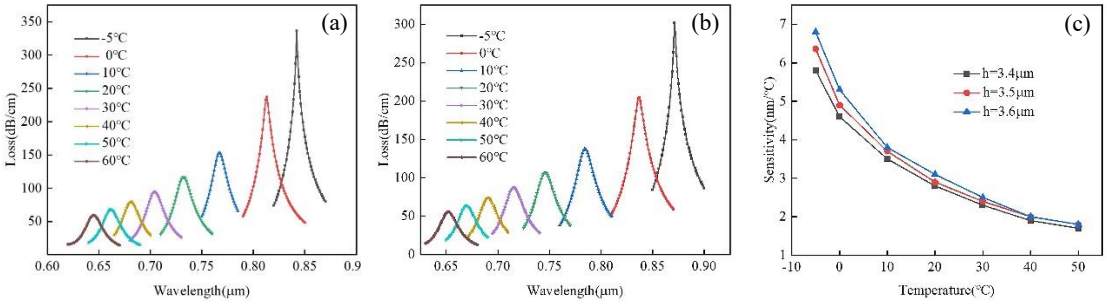

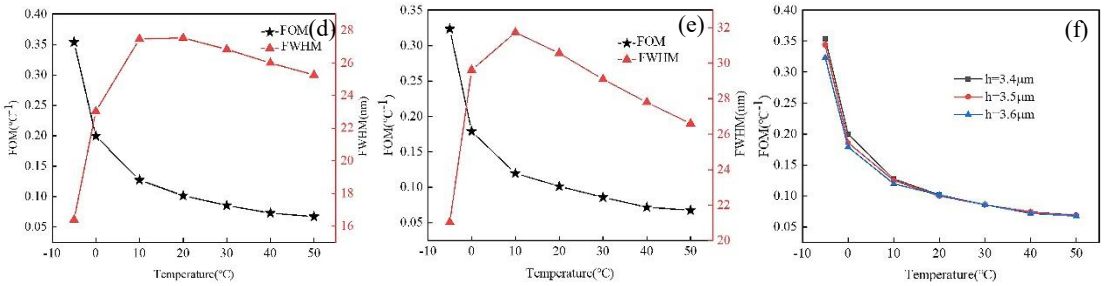

Fig. 7 The core mode loss spectra of (a)h = 3.4 μm and (b) h = 3.6 μm, the (c) sensitivity and (f) FOM versus temperature with different value of h, FOM and FWHM values at (d) h = 3.4 μm and (e) h = 3.6 μm for different temperature

Performance comparison and experimental setup

Table 2 compares the sensing performance among designed and existing PCF temperature sensors. As can be seen from this table, the sensor suggested in this study has superior performance in terms of sensitivity and figure of merit (FOM), as well as a wide temperature detection range of down to -5 °C. In addition, the D-shaped structure efficiently promotes electron excitation on the metal film. As a result, the proposed SPR-PCF temperature sensor exhibits better sensing capabilities than other designs.

Table 2 Sensing performance comparison of various PCF temperature sensors

Structures	Detection range(℃)	Sensitivity(nm/℃)	FOM($℃^{-1}$)	Ref
SPR	20~80	-2.5	-0.061	[7]
LPG	20~50	1.356		[8]
Sagnac interferometer	25~33	1.65		[9]
Coupling between liquid-core mode and defect mode	20~80	-1.9	-0.035	[10]
Bandgap-like effect	20~28	-5.5	0.0762	[11]
Ultracompact	0~100	2.82	0.048	[12]
Polarization-insensitive	20~80	-1.96	-0.272	[13]
SPR	-5~60	6.36	0.3440	This work

The experimental setup of the proposed temperature sensor is shown in Fig. 8. The optical signal is provided by the broadband light source (BBS) transmits into the designed D-shaped PCF through a single-mode fiber (SMF), and then the output spectrum can be observed using an optical spectrum analyzer (OSA), which is connected to the PCF via another SMF. The temperature-sensitive liquid is deposited on the outer layer of the PCF, which is permeable, and the pump controls its inflow and outflow. The temperature controller can adjust the temperature around the sensor. OSA can detect a shift in resonance wavelength at different temperatures when the temperature changes[30].

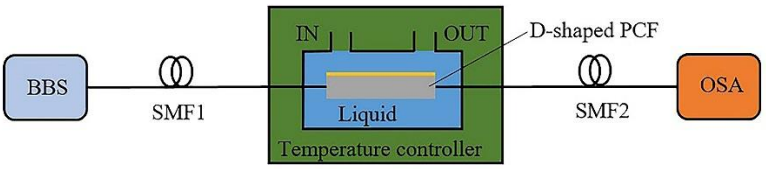

Fig. 8 Schematic diagram of experimental setup for the proposed SPR-PCF temperature sensor

Conclusion

A highly sensitive D-shaped PCF temperature sensor based on SPR is proposed. The D-shaped PCF features an easy-to-manufacture construction and the sensing effect is excellent when the suitable structural parameters are used. The mixture of ethanol and chloroform as the temperature-sensitive liquid, and a slight change in temperature can result in a significant change in its refractive index. The sensing characteristics of the temperature sensor are studied by the finite element method, the results indicate the sensitivity can reach up to 6.36 nm/℃ and the maximum FOM is 0.34396/℃, which are better than existing various types of PCF temperature sensor. Additionally, excellent polynomial fitting is obtained throughout a broad temperature range of -5 °C to 60 °C. The superior performance of the proposed temperature sensor offers a wide range of potential applications in the medical and biochemical fields.

Author Contribution Shutao Wang and Yuhong Lu participated in model design and wrote the main manuscript text. Shutao Wang, Yuhong Lu and Wenbo Ma performed the data analysis and manuscript revisions. Na Liu and Shuanghe Fan prepared figures and tables in the paper. Shutao Wang, Yuhong Lu, Wenbo Ma, Na Liu and Shuanghe Fan discussed the overall research of the proposed temperature sensor.

Funding This work was supported by the National Natural Science Foundation of China (No. 61771419; No. 62173289), and Natural Science Foundation of Hebei Province of China (No. F2017203220).

Availability of Data and Material The datasets analyzed during the current study are available from the corresponding author on reasonable request.

Declarations

Consent for Publication We all the co-authors give the consent for information about the manuscript to be published in Plasmonics.

Conflict of Interest The authors declare no competing interests.

Reference

1. Velázquez-González J S, Monzón-Hernández D, Moreno-Hernández D, Martínez-Piñón F, Hernández-Romano I (2017) Simultaneous measurement of refractive index and temperature using a SPR-based fiber optic sensor. Sensors and Actuators B: Chemical 242:912-920.
2. Lu Y, Wang M T, Hao C J, Zhao Z Q, Yao J Q (2014) Temperature Sensing Using Photonic Crystal Fiber Filled With Silver Nanowires and Liquid. IEEE Photonics J. 6(3):1-7.
3. Sun B, Chen M, Zhou J, Zhang Y (2013) Surface Plasmon Induced Polarization Splitting Based on Dual-Core Photonic Crystal Fiber with Metal Wire. Plasmonics 8(2):1253-1258.
4. Liu Q, Li S, Chen H, Li J, Fan Z (2015) High-sensitivity plasmonic temperature sensor based on photonic crystal fiber coated with nanoscale gold film. Applied physics express 8(4):46701.
5. Du C, Wang Q, Zhao Y, Li J (2017) Highly sensitive temperature sensor based on an isopropanol-filled photonic crystal fiber long period grating. Optical Fiber Technology 34:12-15.
6. Li X, Zhao Y, Zhou X, Cai L (2018) High sensitivity all-fiber Sagnac interferometer temperature sensor using a selective ethanol-filled photonic crystal fiber. Instrumentation science & technology 46(3):253-264.
7. Liu Q, Li S, Chen H, Fan Z, Li J (2015) Photonic Crystal Fiber Temperature Sensor Based on Coupling Between Liquid-Core Mode and Defect Mode. IEEE Photonics J. 7(2):1-9.
8. Peng Y, Hou J, Zhang Y, Huang Z, Xiao R, Lu Q (2013) Temperature sensing using the bandgap-like effect in a selectively liquid-filled photonic crystal fiber. Optics letters 38(3):263-265.
9. Chen H, Li S, Li J, Han Y, Wu Y (2014) High Sensitivity of Temperature Sensor Based on Ultracompact Photonics Crystal Fibers. IEEE Photonics J. 6(6):1-6.
10. Abbasi M, Soroosh M, Namjoo E (2018) Polarization-insensitive temperature sensor based on liquid filled photonic crystal fiber. Optik 168:342-347.
11. Mo X, Lv J, Liu Q, Jiang X, Si G (2021) A Magnetic Field SPR Sensor Based on Temperature Self-Reference. Sensors 21(18):6130.
12. Shuai B, Xia L, Zhang Y, Liu D (2012) A multi-core holey fiber based plasmonic sensor with large detection range and high linearity. Optics express 20(6):5974-5986.
13. Zeng S, Baillargeat D, Ho H P, Yong K T (2014) Nanomaterials enhanced surface plasmon resonance for biological and chemical sensing applications. Chem Soc Rev 43(10):3426-3452.
14. Hinman S S, Mckeating K S, Cheng Q (2017) Surface Plasmon Resonance: Material and Interface Design for Universal Accessibility. Anal. Chem. 90(1):19-39.
15. Peng Y, Hou J, Huang Z, Lu Q (2012) Temperature sensor based on surface plasmon resonance within selectively coated photonic crystal fiber. Applied optics (2004) 51(26):6361.
16. Hameed M F O, Azab M Y, Heikal A M, El-Hefnawy S M, Obayya S S A (2016) Highly Sensitive Plasmonic Photonic Crystal Temperature Sensor Filled With Liquid Crystal. IEEE Photon. Technol. Lett. 28(1):59-62.
17. Han B, Zhang Y, E S, Wang X, Yang D, Wang T, Lu K, Wang F (2019) Simultaneous measurement of temperature and strain based on dual SPR effect in PCF. Optics & Laser Technology 113:46-51.
18. Yi C, Zhang P, Chen F, Dai S, Wang X, Xu T, Nie Q (2014) Fabrication and characterization of Ge20Sb15S65 chalcogenide glass for photonic crystal fibers. Appl. Phys. B 116(3):653-658.
19. Abdullah H, Islam M R, Ahmed K, Malka D, Nguyen T K, Hossain M N, Paul B K, Dhasarathan V

(2020) Theoretical analysis of highly temperature-sensitive fem based optical sensor in the infrared range. Optik 205:164060.
20. Qiu S, Yuan J, Duan S, Zhou X, Mei C, Qu Y, Yan B, Wu Q, Wang K, Sang X, Long K, Yu C (2021) High sensitivity temperature sensor based on a helically twisted photonic crystal fiber. Results in Physics 29:104767.
21. Sharma A K, Gupta B D (2006) Theoretical model of a fiber optic remote sensor based on surface plasmon resonance for temperature detection. Optical Fiber Technology 12(1):87-100.
22. Xu Y, Chen X, Zhu Y (2008) High Sensitive Temperature Sensor Using a Liquid-core Optical Fiber with Small Refractive Index Difference Between Core and Cladding Materials. Sensors 8(3):1872-1878.
23. Zhang Y, Chen H, Wang M, Liu Y, Fan X, Chen Q, Wu B (2021) Simultaneous measurement of refractive index and temperature of seawater based on surface plasmon resonance in a dual D-type photonic crystal fiber. Materials Research Express 8(8):85201.
24. Samoc A (2003) Dispersion of refractive properties of solvents: Chloroform, toluene, benzene, and carbon disulfide in ultraviolet, visible, and near-infrared. Journal of Applied Physics 94(9):6167-6174.
25. Yan X, Fu R, Cheng T, Li S (2021) A Highly Sensitive Refractive Index Sensor Based on a V-Shaped Photonic Crystal Fiber with a High Refractive Index Range. Sensors 21(11):3782.
26. Rifat A A, Mahdiraji G A, Sua Y M, Shee Y G, Ahmed R, Chow D M, Adikan F R M (2015) Surface Plasmon Resonance Photonic Crystal Fiber Biosensor: A Practical Sensing Approach. IEEE Photon. Technol. Lett. 27(15):1628-1631.
27. Chen X, Xia L, Li C (2018) Surface Plasmon Resonance Sensor Based on a Novel D-Shaped Photonic Crystal Fiber for Low Refractive Index Detection. IEEE Photonics J. 10(1):1-9.
28. Wang X, Li S, Chen H, Liu Q, Wang G, Zhao Y (2016) Compatibility of Temperature Sensor and Polarization Filter Based on Au Film and Glycerin Selectively Infilling Photonic Crystal Fibers. Plasmonics 11(5):1265-1271.
29. Islam M S, Sultana J, Rifat A A, Ahmed R, Dinovitser A, Ng B W H, Ebendorff-Heidepriem H, Abbott D (2018) Dual-polarized highly sensitive plasmonic sensor in the visible to near-IR spectrum. Opt. Express 26(23):30347.
30. Rifat A A, Ahmed R, Mahdiraji G A, Adikan F R M (2017) Highly Sensitive D-Shaped Photonic Crystal Fiber-Based Plasmonic Biosensor in Visible to Near-IR. IEEE Sensors J. 17(9):2776-2783.